Prediction on MRAM Etching Endpoint by Response Surface Method

Yan-Yan Ding and Yanfeng Jiang*

Department of Electrical Engineering, School of IoT Engineering, Jiangnan University, Wuxi 214122, China

Abstract: STT-MRAM (Spin-Transfer-Torque Magnetic Random Access Memory) with high-density is considered as one of the most promising storage candidates with potential applications. In the process of MRAM manufacturing, etching step should be stopped precisely at the specific material layer. The dielectric layer should be protected with certain coverage. Then the subsequent etching steps continue. It is crucial to detect the endpoint of the etching during the fabrication process.

In the paper, the factors influencing the etching rate are analysed, including gas pressure, gas temperature, ion sheath thickness, self-biased DC voltage and RF power frequency, respectively. An approach based on Response Surface Method (RSM) is adopted to predict the endpoint of the etching process. The optimized interplay relationship is set up among the gas pressure, the gas temperature, the ion sheath thickness, the self-biased DC voltage and the RF power frequency, *et al.*. It shows that RSM approach is an effective statistical method for the optimization on the etching stop technology, especially when the complex etching condition options are involved. The simulation results demonstrate the MRAM sidewall smoothness can be improved under the optimized etching environment configuration.

Keywords: MRAM, MTJ, RSM, Etching endpoint.

1. INTRODUCTION

When the process technology node keeps shrinking below 45 nm, the existing storage technologies are facing more severe challenges. Magnetic Random Access Memory (MRAM) is the most promising competitor with promising characteristics, including non-volatile, high read-write speed, low power consumption and unlimited durability, *etc.*. As a new generation of MRAM, Spin Torque Transfer (STT)-MRAM shows its excellent scalability and compatibility with CMOS chip manufacturing process, which is expected to be the most promising candidate of the next generation memories. It shows excellent process compatibility and scalability. Its fabrication process can be compatible with CMOS process. When CMOS front-end process is completed, only a few additional masks are needed to complete the MTJ back-end process, without introducing complex processes into CMOS process. However, there are still many challenges, among which high density is the most critical ones, especially for the stand-alone memory. During the fabrication, the etching process plays important role in determining the density of the storage cells in MRAM.

To increase the cell's density in MRAM, in the process of MRAM manufacturing, etching step should be stopped precisely at the specific material layer. The dielectric layer should be protected with certain coverage. Then the subsequent etching steps continue. It is crucial to detect the endpoint of the etching during the fabrication process.

The structure of the paper is as follows. In section II, the methods used in MRAM etching is introduced, focusing on the basic knowledge of ICP etching. Section III introduces the MTJ device's simulation model used in MRAM etching and the parameter settings in TCAD simulation. Section IV introduces the approach of the etching stop time prediction. The influences of multiple variables on the MRAM etch stop time are analysed. Summary and prospects are concluded in Section V.

2. DRY ETCHING PROCESS OF STT-MRAM

Plasma dry etching is widely used in MTJ etching process. Reactive Ion Etching (RIE) is used to prepare high-quality MTJ device (Endoh *et al*., 2018; Xue *et al*., 2014). However, with the continuous reduction of process technology node, the shortcomings of RIE etching are gradually exposed. With single RF power supply in RIE system, it is impossible to achieve low etching damage while maintaining etching rate. In addition, the gas pressure in the etching chamber is relative high, while the generated plasma density is relative low, resulting in poor control on the etching morphology.

Inductive Coupled Plasma (ICP) etching system shows better performance than the traditional RIE syste. In the ICP system, two independent RF sources are included, and the generated plasma density is relative high. The investigated ICP system is shown Figure **1**. It can achieve high etching rate and low etching damage with low etching pressure. Garay A and LeeT Y realized high-density etching of MRAM with ICP etching system, respectively (Garay *et al*., 2015; Lee *et al*., 2013).

* Address correspondence to this article at the Department of Electrical Engineering, School of IoT Engineering, Jiangnan University, Wuxi 214122, China; Tel: +86-13520063323; E-mail: jiangyf@jiangnan.edu.cn

E-ISSN: 2409-9848/23

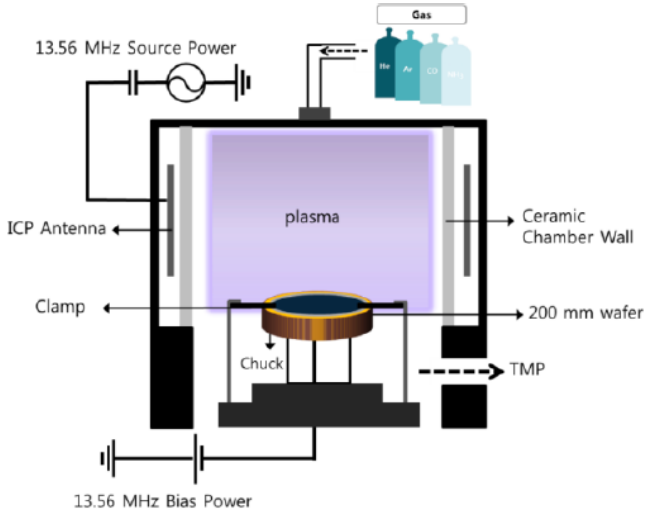

Figure 1: Schematic of ICP etching system.

Figure **2** shows the process flow of plasma etching by taking CF_4 etching silicon as an example in the paper. The plasma etching is usually conducted in the following four steps (Nojiri, 2015): The first step is the plasma generation under the applied electric field. Then the plasma is transported and adsorbed on the etched target. Thirdly, the reaction is occurred on the surface of the target. The surface would be etched and the etched products could be produced. Finally, the etched products are released from the surface.

During the etching process, with the electrode negatively biased, the electrons are pushed away from the negative electrode. The region near the electrode is called 'ion sheath' since there isn't any electron. In the ion sheath, only ions exist inside. Since the electron density in this region is very low, the probability of collision excitation is very low and there is almost no light emission. Therefore, the ion sheath is also called 'dark space' (Donnelly & Kornblit, 2013) .

Figure **3** shows the potential distribution inside the etching chamber (Cardinaud *et al*., 2000). The plasma is conductive on the micro level, while equi-potential on

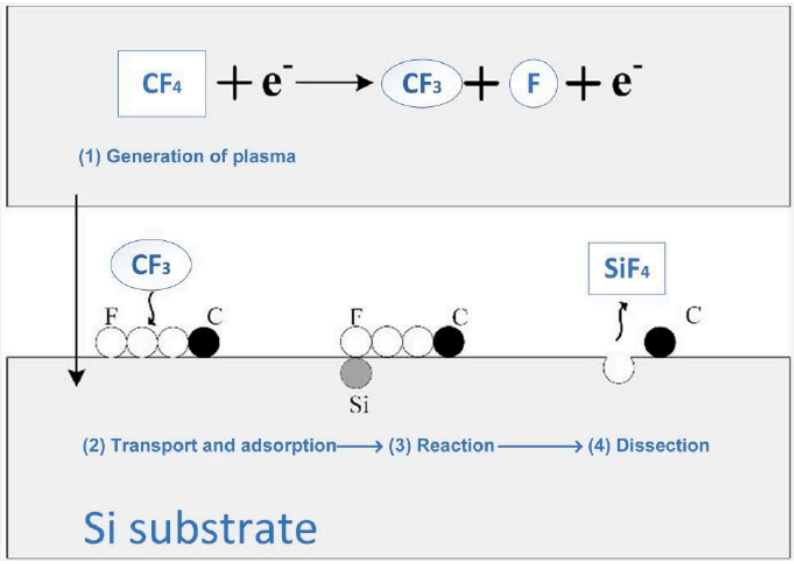

Figure 2: Plasma etching process, taking CF4 etching silicon as an example.

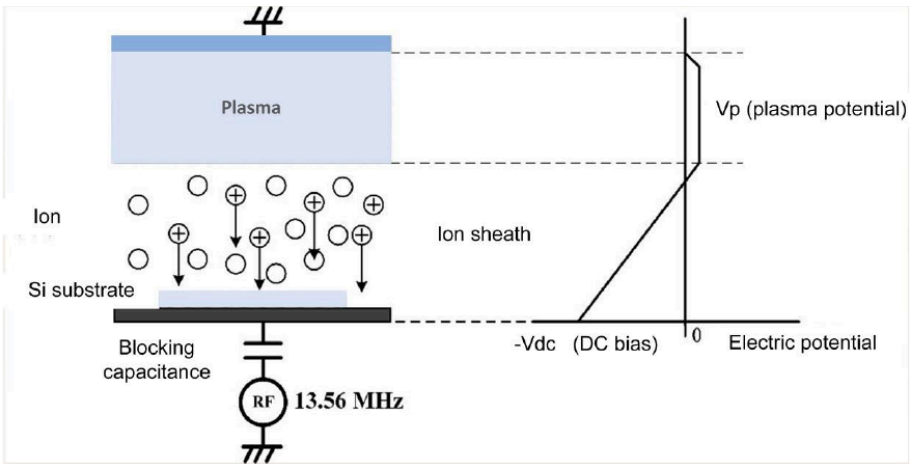

Figure 3: Typical structure of plasma etching chamber.

the macro level. The potential of plasma is called plasma potential V_P. At the interface between the plasma and the ion sheath, with the assistance of Vdc, the ions can be accelerated to the surface of the wafer. Here, the energy obtained by ions is equivalent to $| V_P | + | V_{DC} |$.

3. SIMULATION MODEL OF MTJ DEVICE

TCAD process simulator can provide the simulation ability of a series of semiconductor production processes, such as CMOS process and MTJ processes such as film deposition, plasma etching, chemical mechanical polishing and so on(Ma *et al*., 2010). At the same time, due to the particularity of magnetic materials, the preparation of MRAM has extremely strict requirements on experimental equipment and experimental conditions. Therefore, the feasibility of the optimization scheme is verified by theoretical analysis and simulation experiments. We will study the MRAM etching process based on TCAD in this section.

TCAD provides physical and numerical two-dimensional simulation capability for the semiconductor process, which is helpful for the development of the device process and the optimization of the semiconductor manufacturing process. The numerical calculation is based on a series of physical models and mathematical equations, which are based on the theories of solid state physics and semiconductor physics or some empirical formulas.

In TCAD system, Elite module provides a series of etching models, corresponding to different etching technologies (Neureuther *et al*., 1979; Reynolds *et al*., 1979; Takagi *et al*., 2002). Elite allows the usage of complex models for deposition and etching processes. In addition, Elite has Monte Carlo deposition, Monte Carlo etching and chemical mechanical polishing (CMP) modules. The user can establish the etching model by defining a machine or calling the default machine. The established etching model can be used to simulate the deposition and etching process. The adopted machine in the model can be modified. So different process requirements can be satisfied by the adjustments of the machine parameters.

Using plasma etching, the Elite module can provide relevant parameters required for plasma etching, mainly including the following aspects. The first part is the parameter settings of the etching gas and the reaction ion, as shown in Table **1**. The second part is the definition of etching rate parameters, as shown in Table **2**. The parameter definitions of the etching equipment are listed in Table **3**. The definitions of the model parameters are shown in Table **4**.

Table 1: Parameters of Etching Gas and Reactive Ions

Parameter	Default Value
Plasma etching chamber pressure	10 mTorr
Gas temperature in etching chamber	300 K
Reaction ion temperature in etching chamber	300 K
Atomic mass of gas	40
Atomic mass of reaction ion	40
Particle number of ion flux used for MC calculation	10,000

Table 2: Etching Rate Parameters

Parameter	Default Value
Linear coefficient K.I of plasma etching rate related to ion flux	0~1
Linear coefficient K.F of plasma etching rate related to chemical flux	0~1
Linear coefficient K.D of plasma etching rate related to deposition flux	0~1

Table 3: Parameters of Etching Equipment

Parameter	Default Value
DC bias voltage in ion sheath	32.5 V
RF power frequency	13.56 MHz
Ion sheath thickness	mm

Table 4: Model Parameters

Parameter	Default Value
Calculation model of voltage drop in ion sheath Constant model	CONSTANT
Surface dynamics model	ER.LINER

In the MRAM etching process, poor etching morphology always exists on the etched structure. Because of the problem of the transportation of the etched products, the bottom adhesion caused by etching deposition can be observed and is the key aspect on the influence of the density.

Figure **4** shows the schematic structure of the etched MTJ stack layers. During the etching process, Ar ion beam is ionized and accelerated in the reaction chamber, and then irradiates the wafer below to selectively etch the area not covered by the hard mask.

Based on the current etching process, it is very difficult to fabricate the MTJ nano cells with steep sidewall edges while completely avoiding sidewall re-deposition and magnetic layer corrosion. The re-deposition phenomenon on the sidewall of the MTJ

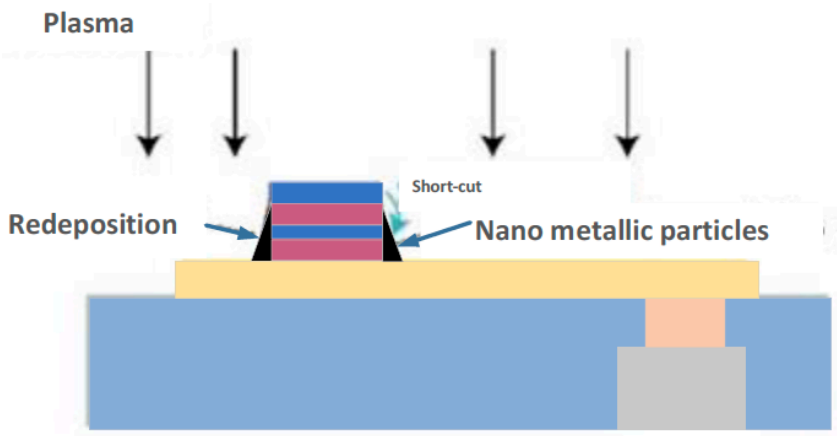

Figure 4: Schematic of the etched MTJ device, showing the influences of the etching process, including the redeposition, the short-cut by the produced nano metallic particles.

device may seriously deteriorate the electrical performance of MTJ devices, and even lead to barrier short-cut defect, as shown in Figure **4**.

In order to reduce the impact of re-deposition, in the sidewall etching step of halogen based dry etching technology, it is necessary to rotate and/or tilt the wafer during the etching process. In addition, the shadow effect should be considered, which refers to the impact caused by the insufficient spacing between the MTJ devices and the limited etching coverage at the lower corner of MTJ contour. To get the high-density array integration, all these problems during the etching process should be solved.

The device structure used in the simulation is shown in Figure **5**, in which Figure **5**(**a**) shows the planar MTJ structure, while Figure **5**(**b**) shows the vertical MTJ device (X. Zhang *et al*., 2020).

In order to optimize the etching effect, we adopt the following etching scheme as shown in Figure **6**.

4. PREDICTION OF ETCHING RATE AND ETCHING END POINT OF MRAM

In the MRAM etching process, the etching needs to be terminated at a specific material layer. How to determine the etching endpoint is really critical to the quality of the MTJ device and the high-density integration of MRAM. It is necessary to design a prediction scheme for the stop end point of high-density MRAM etching. In this section, the etching conditions affecting the etching rate of MRAM are analysed.

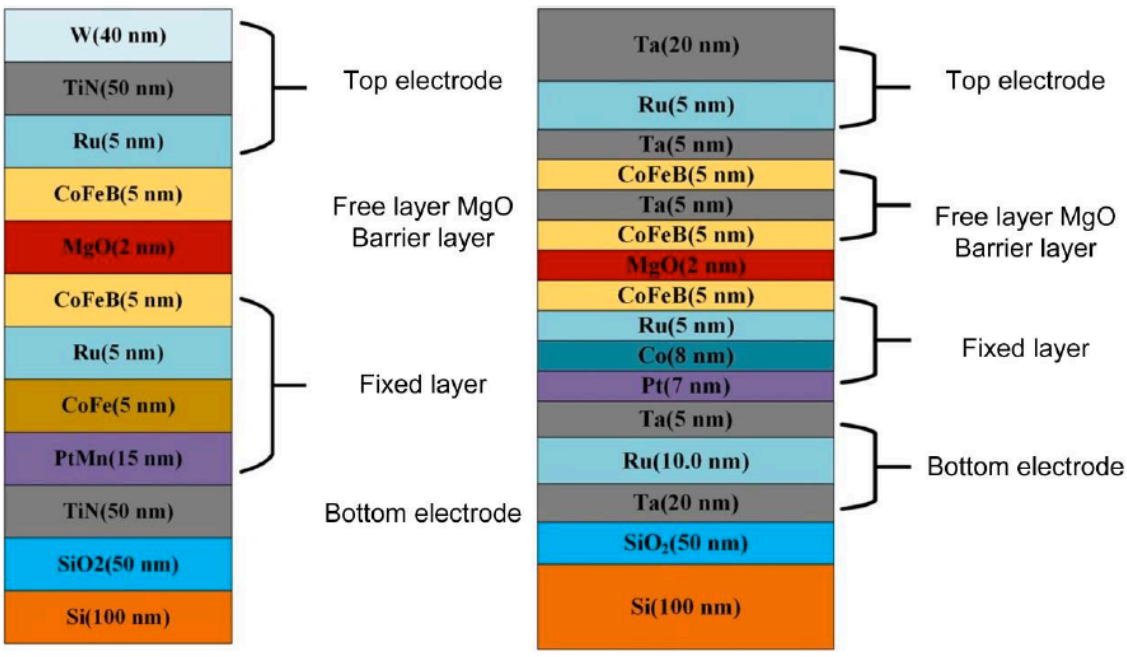

(**a**) Planar MTJ (**b**) Vertical MTJ

Figure 5: Device structure and device parameter definition.

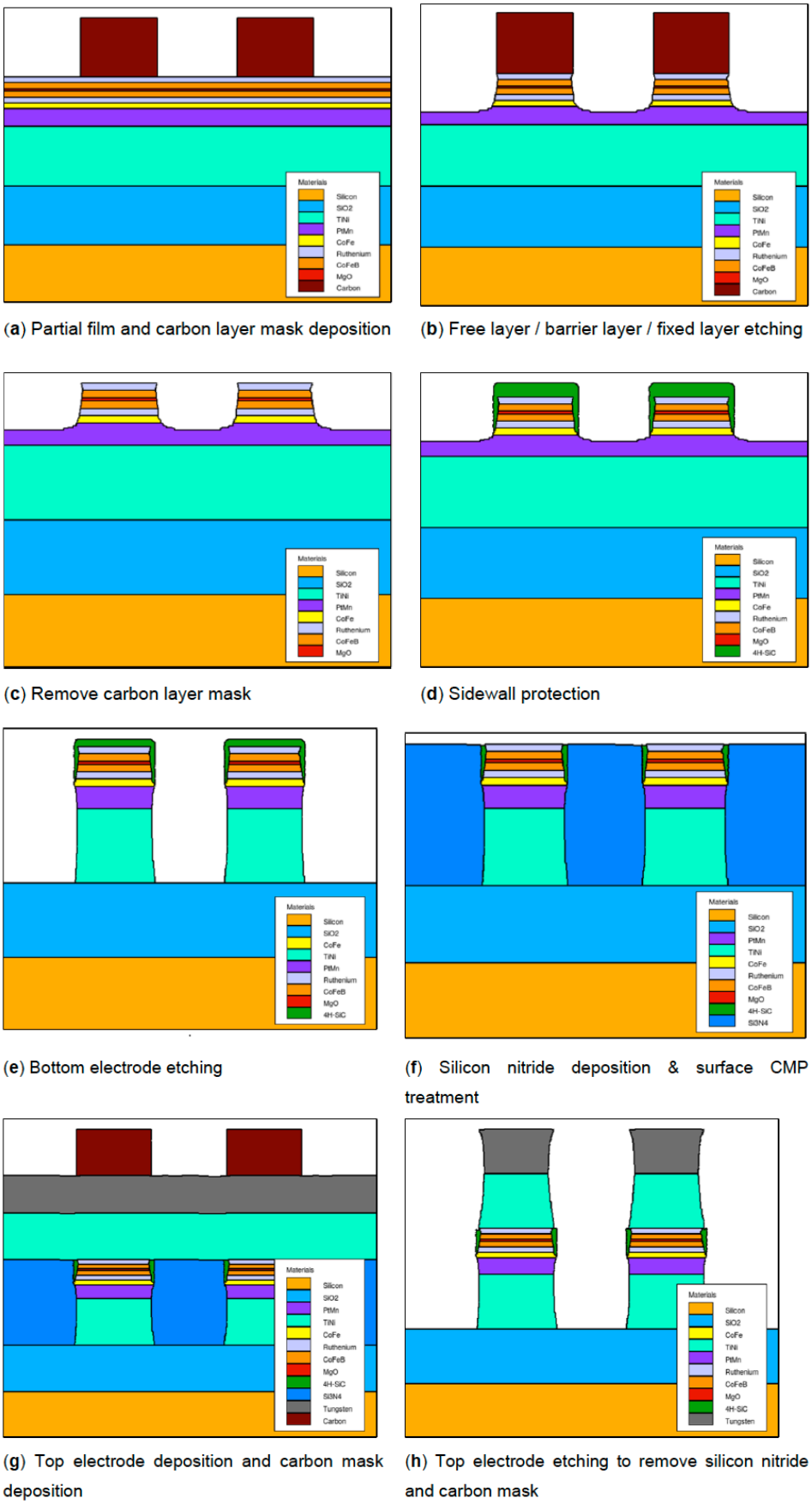

(**a**) Partial film and carbon layer mask deposition

(**b**) Free layer / barrier layer / fixed layer etching

(**c**) Remove carbon layer mask

(**d**) Sidewall protection

(**e**) Bottom electrode etching

(**f**) Silicon nitride deposition & surface CMP treatment

(**g**) Top electrode deposition and carbon mask deposition

(**h**) Top electrode etching to remove silicon nitride and carbon mask

Figure 6: Simulation flow chart of optimized etching process.

Based on the analysis, the prediction scheme on the etching-stop point of STT-MRAM is proposed.

4.1. Parameter Setting of MRAM Plasma Etching

According to the Elite module mentioned in section

III, five variables are chosen in the paper to study the effects of different variables on the etching rate of MTJ device. The chosen variables include RF frequency, self bias voltage, ion sheath thickness, gas pressure and gas temperature in the reaction chamber.

Figure **7** shows the effect of the gas pressure in the reaction chamber on the etching rate. When the gas pressure is 10 mTorr, the bottom electrode of the MTJ device is engraved firstly. At the same time, compared with the gas pressure of 50 mTorr, the etching rate of the bottom electrode is faster. The reason is that the gas pressure directly affects the average free path of the ions. The lower gas pressure enables the ions to obtain a longer average free path, which directly leads to less ion collision probability in the ion sheath. Therefore, the ions in the sheath are accelerated under low pressure. Thus the probability of collision and scattering with gas molecules is reduced, showing stronger directional consistency, to improve the etching rate.

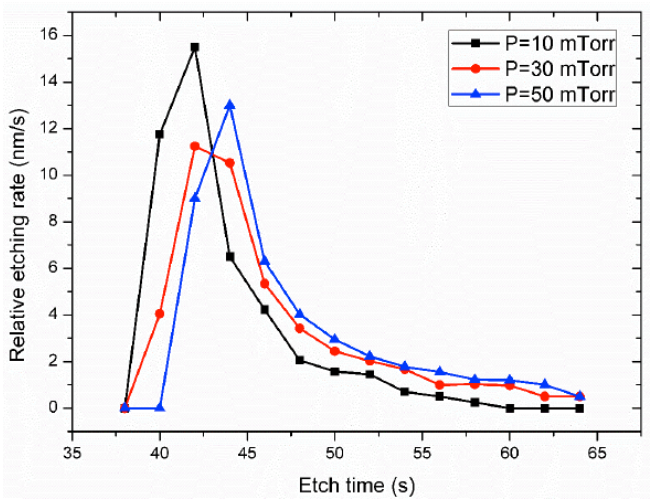

Figure 7: Effect of gas pressure on bottom etching rate.

Figure **8** shows the influence of the gas temperature on the etching rate. The average free path of the ions is directly proportional to the gas temperature. With the increment of the gas temperature in the chamber, the bottom electrode is etched firstly. The average free path is increased with the temperature increasing, which is helpful for the improvement of the directivity of ions and the consequent etching rate.

The average free path refers to the distance that a particle passes from one collision to the next ones. It is the distance that a particle can travel without collision. The average free path is mainly affected by the gas pressure and the gas temperature. The equation is as follows(Jennings, 1988):

$$\lambda = \frac{K_B T}{\sqrt{2}\pi d^2 P} \quad (1)$$

where d the effective diameter of the molecule, P the gas pressure, K_B the Boltzmann constant, and T the temperature.

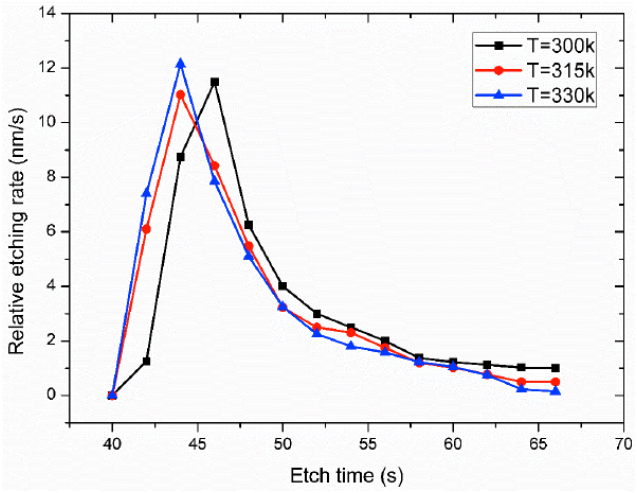

Figure 8: Effect of gas temperature on bottom etching rate.

In the chamber with lower pressure and higher temperature, there are fewer molecules in the gas. The collision probability with the ions is very low. So the average free path is longer. The average free path is inversely proportional to the gas pressure, while proportional to the temperature in the chamber.

The ion sheath thickness is affected by multiple variables. Figure **9** shows the influence of ion sheath thickness on the MTJ etching rate, with the thickness of 5 mm, 3 mm and 1 mm, separately. When the thickness of ion sheath is reduced from 5 mm to 1 mm, the etching rate becomes faster, and the spacing between the bottom electrodes tends to be stable. With the sheath thickness 5 nm, the duration etching time for the stable space of the bottom electrode is around 8 seconds. The influence of the ion sheath thickness on the bottom etching rate is negatively correlated. Smaller ion sheath thickness is helpful for the improvement of the etching rate.

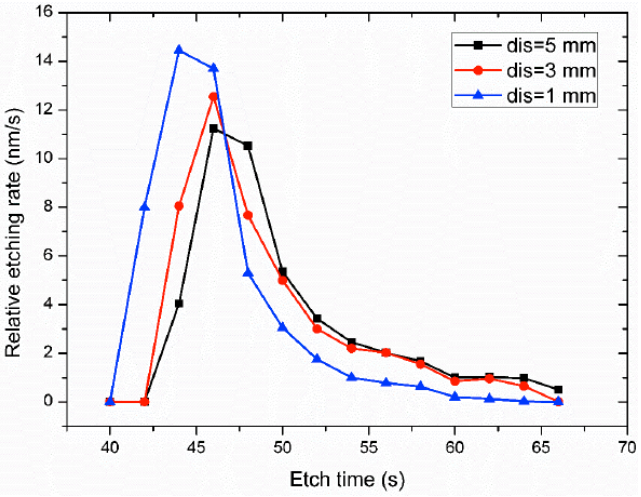

Figure 9: Effect of ion sheath thickness on bottom etching rate.

To participate in the etching process, the ions need to pass through the ion sheath, and be accelerated by the electric field. The accelerated ions land on the surface of the material with high energy, and participate in the reaction after being adsorbed on the material surface. In the scope of the ion sheath, ions have the possibility of collision scattering with each other and affect the direction of ion emission. The probability of the ion scattering in the ion sheath mainly depends on the relationship between the thickness of the ion sheath and the average free path of the ion.

Ion sheath thickness d_{is} can be expressed by Child-Langmuir equation(Barnes *et al*., 1991) :

$$d_{is} = \frac{2}{3}\left(\frac{\varepsilon_0}{i_{io}}\right)^{\frac{1}{2}}\left(\frac{2e}{m_i}\right)^{\frac{1}{4}}(V_P - V_{dc})^{\frac{3}{4}} \quad (2)$$

where I_{io} the ion current density, ε_0 the dielectric constant of vacuum, e the amount of charge, m_i the ionic mass, V_P the plasma potential and V_{dc} the DC self bias voltage.

In addition to the influence of the ion directivity on the etching effect, the ion energy also plays important role in etching. The factors affecting ion energy and ion directivity are often intertwined. When the ions pass through the ion sheath, the collision scattering changes not only the emission direction of the ions, but also the transferred energy of the ions in the collision (Y. Zhang *et al*., 2015).

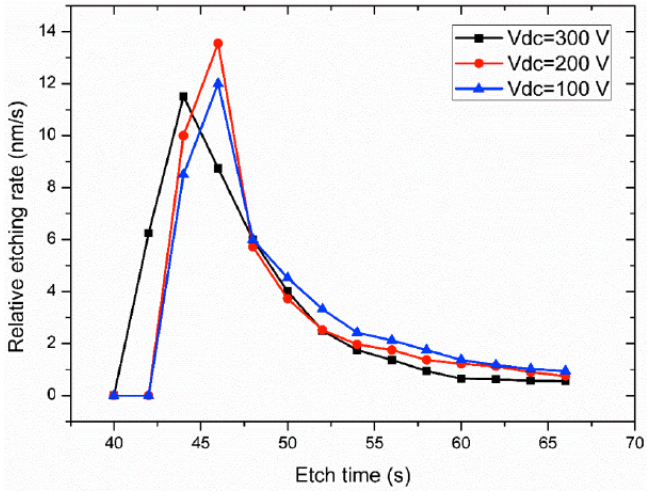

Figure 10: Effect of DC bias voltage on bottom etching rate.

Figure **11** shows the effect of the self biased DC Voltage V_{dc} on the etching rate. With the voltage decreasing, the ion strength through electric field and the ion energy obtained by positive ions through electric field acceleration are also decreased. Therefore, when V_{dc} = 100 V, it needs more etching time. To obtain the vertical wall profile, a large DC bias voltage is required. However, some negative effects are aroused by the large DC bias voltage. For example, the hard mask adopted in the etching process would be etched with the increased etching rate. Also the large DC bias voltage could introduce the etching damage by the ion bombardment with high energy. The surface roughness on the etched layer would be increased accordingly.

Figure **11** shows the influence of RF frequency on the etching effect. With the RF frequency 13.56 MHz, the etching rate is low. With the frequency 3.56 MHz, the etching rate is increased, resulting in a reduction in the time required for etching. The frequency of 13.56 MHz is generally used by default for plasma etching equipment.

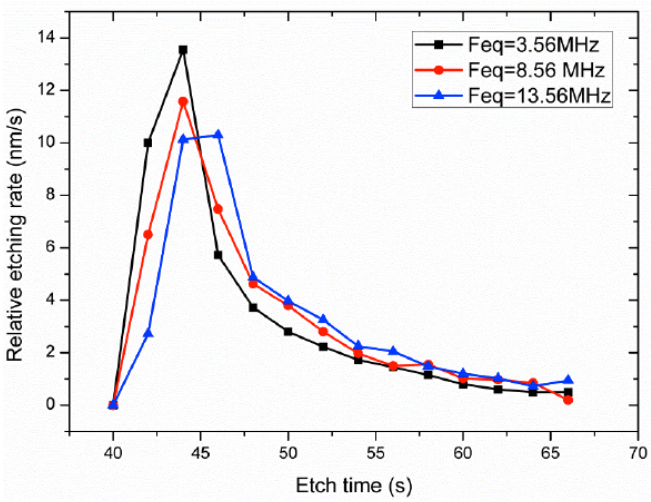

Figure 11: Effect of RF frequency on bottom etching rate.

4.2. RSM Model on Etching Endpoint Prediction

Figure **12** shows the etching stop time under different variable changes. To analyze the interplayed relationship, RSM model is used to discuss the change of stopping time. The establishment process of RSM model is shown in Figure **13**.

RSM model is a multi-dimensional model analysis method proposed by British scholar Box & Wilson in 1951(Draper, 1992). The purpose of this analysis method is to express the response surface of the dependent variable when two or more independent variables change. It can express the relationship between multiple input variables and the corresponding output. It has been successfully applied in many fields such as industry and agriculture(Gunst, 1996; Kim & Na, 1997).

Specifically, it uses polynomials to fit arbitrary functions, such as natural exponential functions can be express by Taylor expansion as:

$$e^x = 1 + x + \frac{x^2}{2!} + \frac{x^3}{3!} + \frac{x^4}{4!} + \quad (3)$$

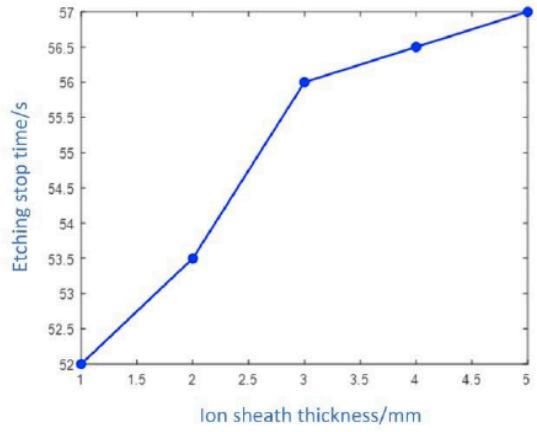

(a) Relationship between ion sheath thickness and etching stop time

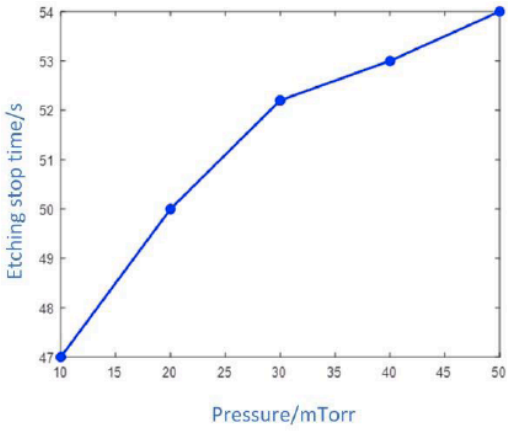

(b) Relationship between gas pressure and etching stop time

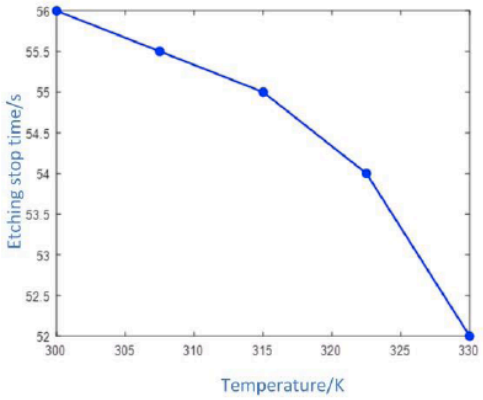

(c) Relationship between gas temperature and etching stop time

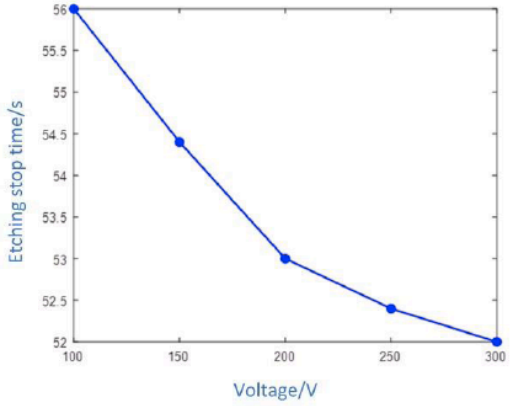

(d) Relationship between self-bias voltage and etching stop time

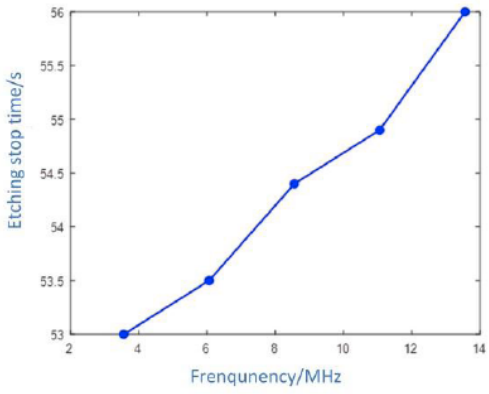

(e) Relationship between RF frequency and etching stop time

Figure 12: Variation trend of etching stop time under different conditions.

which can be generally represented by:

$$y = \beta_0 + \sum_{i=1}^{k} \beta_i x_i + \varepsilon \quad (4)$$

That is the expression of one-dimensional array, generalized to two-dimensional and n-dimensional array is:

$$y = \beta_0 + \sum_{i=1}^{m} \beta_i x_i + \sum_{i=1}^{m} \beta_{ii} x_i x_{j+} \sum \sum_{i<j} \beta_{ij} x_i x_{j+} \varepsilon \quad (5)$$

$$y_i = \beta_0 + \sum_{j=1}^{k} \beta_i x_{ij} + \varepsilon_i \; i = 1,2,\ldots,n \quad (6)$$

For natural exponential functions, when the polynomial reaches to three times, it becomes very close to the actual function in range of [0,1], which indicates we can fit the function with a polynomial that is easier to handle.

$$y = X\beta + \varepsilon \quad (7)$$

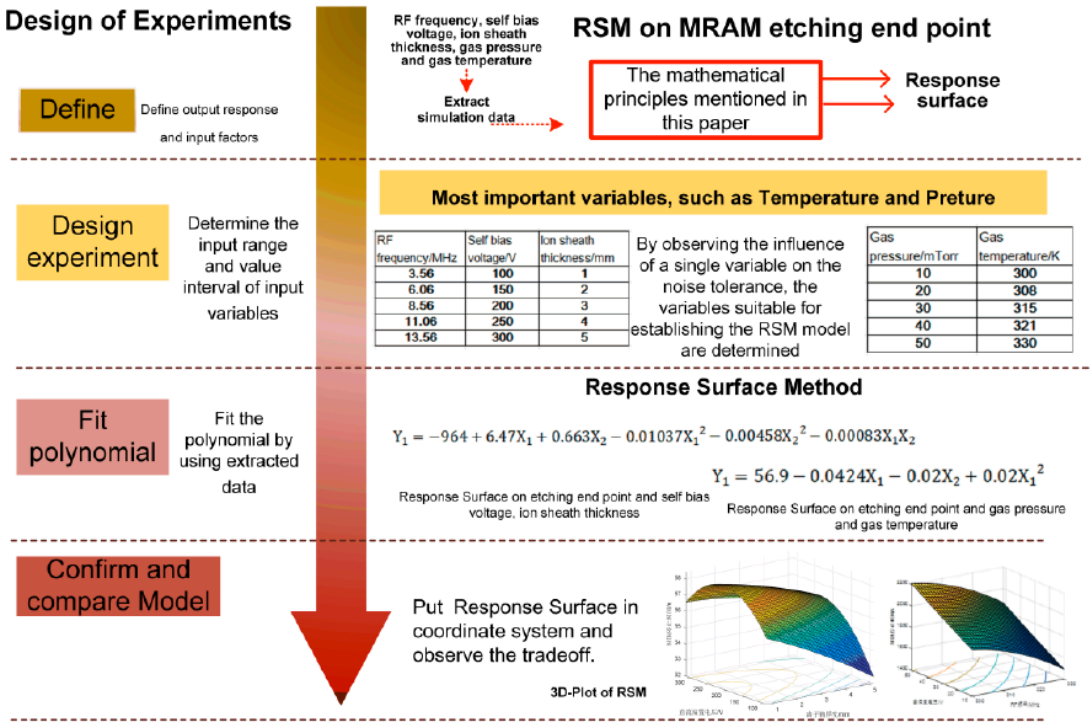

Figure 13: Process of building RSM model on MRAM etching-stop point.

Among them

$$y=\begin{bmatrix} y_1 \\ y_2 \\ \vdots \\ y_n \end{bmatrix} \quad X=\begin{bmatrix} 1 & x_{11} & x_{12} \cdots & x_{1k} \\ 1 & x_{21} & x_{22} \quad \cdots & x_{2k} \\ \vdots & \vdots & \vdots \quad \vdots & \vdots \\ 1 & x_{n1} & x_{n2} \cdots & x_{nk} \end{bmatrix}$$

$$\beta=\begin{bmatrix} \beta_0 \\ \beta_1 \\ \vdots \\ \beta_k \end{bmatrix} \quad \varepsilon=\begin{bmatrix} \varepsilon_0 \\ \varepsilon_1 \\ \vdots \\ \varepsilon_k \end{bmatrix}$$

Minimum variance is derived as:

$$L=\sum_{i=1}^{n}{\varepsilon_i}^2=\varepsilon'\varepsilon=(y-X\beta)'(y-X\beta) \tag{8}$$

Find the differential function of above variance and make result equal to 0:

$$\frac{\partial L}{\partial \beta}\Big|_{\hat{\beta}}=-2X'y+2X'X\,\hat{\beta}=0 \tag{9}$$

According to formula above, we can derive value of $\hat{\beta}$:

$$\hat{\beta}=(X'X)^{-1}X'y \tag{10}$$

To substitute it into the original equation, we can fit a function by some polynomial functions.

$$\hat{y}=X\hat{\beta} \tag{11}$$

The goal of RSM model is to find the quantitative relationship between the response indicators and each factor. To find the best combination of each factor, data on the basis of multiple linear regression should be actively collected to obtain regression equations with better properties. The complex multi-dimensional space surface established is closer to the actual situation. RSM was already widely used in different industries such as navigation or food chemistry(Yu-Xiang *et al*., 2010). Here we apply it to optimization of MRAM ICP process, as shown in Figure **14**(**a**) is the RSM model with ion sheath thickness and self-bias voltage.

$$Y_1=-964+6.47X_1+0.663X_2-0.01037{X_1}^2-0.00458{X_2}^2-0.00083X_1X_2 \tag{12}$$

where X_1 the ion sheath thickness (Unit: mm), X_2 he self-bias voltage (Unit: V). Figure **14**(**b**) shows the RSM model with ion RF frequency and self-bias voltage.

$$Y_2=56.9-0.0424X_1-0.02X_2+0.02{X_1}^2 \tag{13}$$

where X_1 the ion RF frequency (Unit: MHz), X_2 the self bias voltage (Unit: V).

After sorting out the simulation data and the influence of the equipment parameter on etching stop time, the RSM model is established as follows, and its mathematical expression is as follows.

$$Y_3=61.57-0.907X_1-0.0082X_2-0.723{X_3}^2+0.069{X_1}^2+0.000003{X_2}^2$$
$$+0.0344{X_3}^2+0.00229X_1X_2+0.0167X_1X_3-0.000333X_2X_3 \tag{14}$$

where X_1 is the ion sheath thickness (Unit: mm), X_2 the self bias voltage (Unit: V), and X_3 the RF frequency (Unit: MHz).

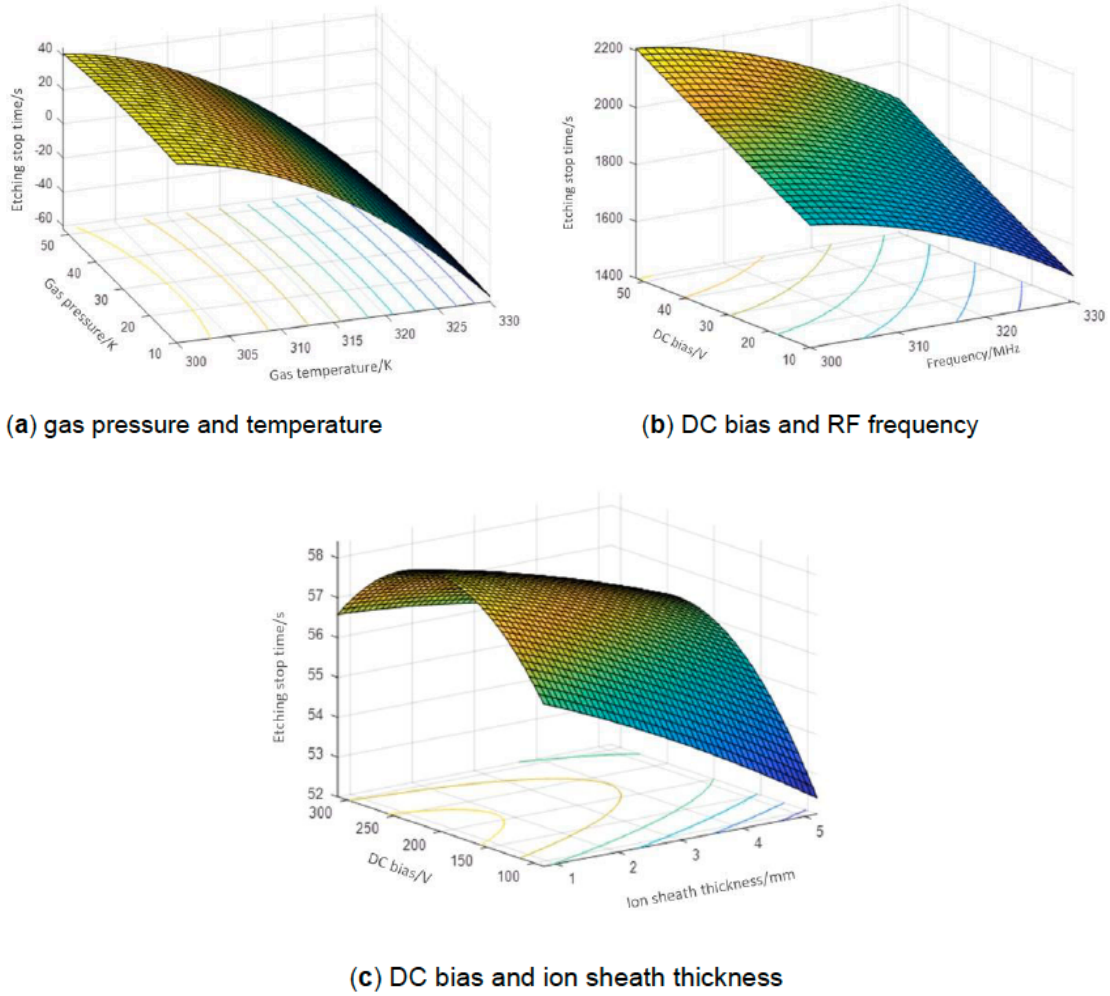

Figure 14: Relationship between different parameters and etching stop time.

Through these fitting formulas, the approximate range of etching stop time under different conditions can be predicted, which can provide strong guidance for the etching process.

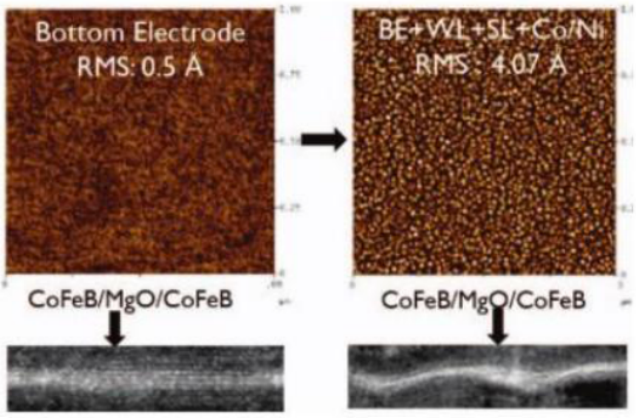

Figure 15: TEM images of CoFeB/MgO/CoFeB deposited on respective surfaces on BEC(Kar, G.S,2014).

Since the smoothness of the interlayer interface is the key to improve TMR value, CMP machining is usually used to minimize the surface roughness. If accurate etching-stop time prediction can be achieved during the etching process, over etching or insufficient etching can be avoided. Accurate prediction of the etching-stop time can improve the smoothness of the etching surface and the etching sidewall angle. The bottom electrode roughness is usually characterized by RMS (Kar, G.S,2014). Figure **15** shows the images of atomic force microscope and high-resolution transmission electron microscope. The interface roughness is increased from 0.5 μ m to 4.07 μ m, resulting in significant TMR degradation.

In addition to the etching-stop time, the selection of etching gas also has an impact on the etching effect. For example, the etching angle of He gas in the paper is superior to other etching gases as shown in Figure **16** (Yang, K. C, 2017).

5. SUMMARY AND PROSPECT

In this paper, RSM approach is adopted to analyze the interplayed variables that influence the dry etching profiles during MRAM fabrication. The effects of five variables on etching rate are studied by TCAD simulation, and the physical mechanism is discussed.

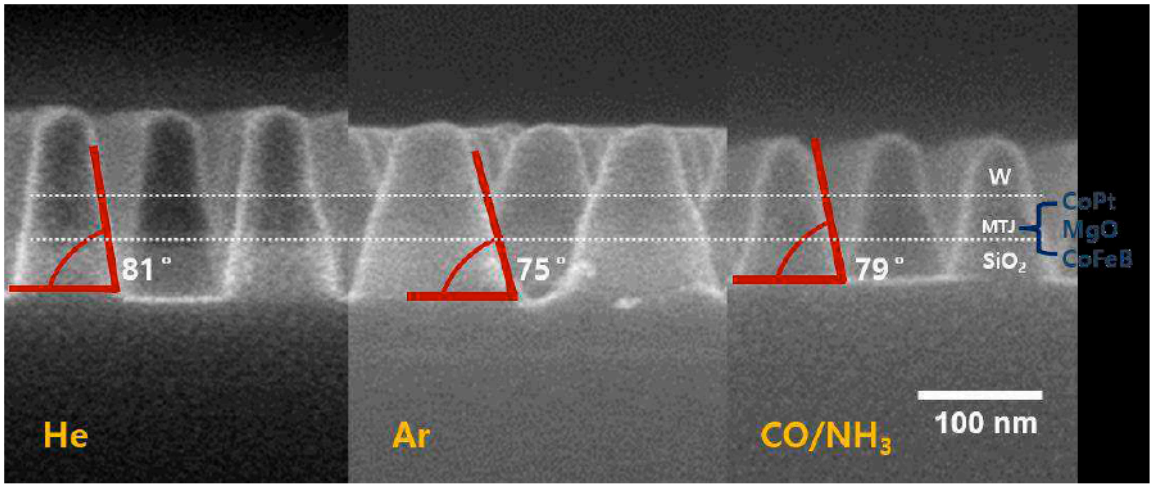

Figure 16: SEM images of the etched MTJ patterns etched using different gases(Yang, K. C, 2017).

This paper also analyzes the variation trend of MRAM etching stop time under the joint influence of different variables based on the established RSM model. The RSM polynomial model accuracy provides a reference for improving the etching rate and predicting the etching stop time. The established RSM model has potential application in the dry etching process of MRAM fabrication to improve its quality.

REFERENCE

[1] Barnes, M. S., Forster, J. C., & Keller, J. H. (1991). Ion kinetics in low-pressure, electropositive, RF glow discharge sheaths. IEEE Transactions on plasma science, 19(2), 240-244. https://doi.org/10.1109/27.106819

[2] Cardinaud, C., Peignon, M. C., & Tessier, P.-Y. (2000). Plasma etching: principles, mechanisms, application to micro-and nano-technologies. Applied Surface Science, 164(1-4), 72-83. https://doi.org/10.1016/S0169-4332(00)00328-7

[3] Donnelly, V. M., & Kornblit, A. (2013). Plasma etching: Yesterday, today, and tomorrow. Journal of Vacuum Science & Technology A: Vacuum, Surfaces, and Films, 31(5), 050825. https://doi.org/10.1116/1.4819316

[4] Draper, N. R. (1992). Introduction to Box and Wilson (1951) on the experimental attainment of optimum conditions (Breakthroughs in Statistics (pp. 267-269). Springer. https://doi.org/10.1007/978-1-4612-4380-9_22

[5] Endoh, T., Kang, S., Kudo, T., & Yagi, Y. (2018). Etch Process Technology for High Density STT-MRAM. (Ed.),^(Eds.). 2018 IEEE International Magnetics Conference (INTERMAG). https://doi.org/10.1109/INTMAG.2018.8508858

[6] Garay, A. A., Choi, J. H., Hwang, S. M., & Chung, C. W. (2015). Inductively coupled plasma reactive ion etching of magnetic tunnel junction stacks in a CH3COOH/Ar gas. ECS Solid State Letters, 4(10), P77. https://doi.org/10.1149/2.0071510ssl

[7] G.S. Kar; W. Kim; T. Tahmasebi; J. Swerts; S. Mertens; N. Heylen; T. Min(2014). Co/Ni based p-MTJ stack for sub-20nm high density stand alone and high performance embedded memory application," 2014 IEEE International Electron Devices Meeting, 2014, pp. 19.1.1-19.1.4.

[8] Gunst, R. F. (1996). Response surface methodology: process and product optimization using designed experiments. Taylor & Francis. https://doi.org/10.2307/1270613

[9] Jennings, S. (1988). The mean free path in air. Journal of Aerosol Science, 19(2), 159-166. https://doi.org/10.1016/0021-8502(88)90219-4

[10] Kim, S.-H., & Na, S.-W. (1997). Response surface method using vector projected sampling points. Structural safety, 19(1), 3-19. https://doi.org/10.1016/S0167-4730(96)00037-9

[11] Lee, T. Y., Lee, I. H., & Chung, C. W. (2013). Inductively coupled plasma reactive ion etching of magnetic tunnel junction stacks using H2O/CH4 mixture. Thin Solid Films, 547, 146-150. https://doi.org/10.1016/j.tsf.2013.04.022

[12] Ma, T., Moroz, V., Borges, R., & Smith, L. (2010). TCAD: Present state and future challenges. (Ed.),^(Eds.). 2010 International Electron Devices Meeting. https://doi.org/10.1109/IEDM.2010.5703367

[13] Neureuther, A., Liu, C., & Ting, C. (1979). Modeling ion milling. Journal of Vacuum Science and Technology, 16(6), 1767-1771. https://doi.org/10.1116/1.570290

[14] Nojiri, K. (2015). Dry etching technology for semiconductors. Springer. https://doi.org/10.1007/978-3-319-10295-5

[15] Reynolds, J. L., Neureuther, A. R., & Oldham, W. G. (1979). Simulation of dry etched line edge profiles. Journal of Vacuum Science and Technology, 16(6), 1772-1775. https://doi.org/10.1116/1.570291

[16] Takagi, S., Iyanagi, K., Onoue, S., Shinmura, T., & Fujino, M. (2002). Topography simulation of reactive ion etching combined with plasma simulation, sheath model, and surface reaction model. Japanese journal of applied physics, 41(6R), 3947. https://doi.org/10.1143/JJAP.41.3947

[17] Xue, L., Nistor, L., Ahn, J., Germain, J., Ching, C., Balseanu, M., Trinh, C., Chen, H., Hassan, S., & Pakala, M. (2014). A self-aligned two-step reactive ion etching process for nanopatterning magnetic tunnel junctions on 300 mm wafers. IEEE Transactions on Magnetics, 50(11), 1-3. https://doi.org/10.1109/TMAG.2014.2322351

[18] Yang, K.C., Park, S.W., Lee, H.S., Yeom, G.Y.(2017). Nanoscale Spin-Transfer Torque MRAM Etching Using Various Gases. ECS Transactions, 77(29-36). https://doi.org/10.1149/07703.0029ecst

[19] Yu-Xiang, Z., Hui-Ge, Q. U., Run-Ya, Y., Bo, Y. U., Huan, S., & Hua-Kai, S. (2010). Application of RSM to Microwave-assisted Extraction Optimization of Flavanoids from Blueberry Leaves. Food Science.

[20] Zhang, X., Zhang, G., Shen, L., Yu, P., & Jiang, Y. (2020). Life-time degradation of STT-MRAM by self-heating effect with TDDB model. Solid-State Electronics, 173, 107878. https://doi.org/10.1016/j.sse.2020.107878

[21] Zhang, Y., Kushner, M. J., Sriraman, S., Marakhtanov, A., Holland, J., & Paterson, A. (2015). Control of ion energy and angular distributions in dual-frequency capacitively coupled plasmas through power ratios and phase: Consequences on etch profiles. Journal of Vacuum Science & Technology A: Vacuum, Surfaces, and Films, 33(3), 031302. https://doi.org/10.1116/1.4915248

Received on 03-04-2023 Accepted on 18-05-2023 Published on 24-05-2023

DOI: https://doi.org/10.31875/2409-9848.2023.10.06